Chinese Chemical Letters 35 (2024) 109379

Contents lists available at ScienceDirect

Chinese Chemical Letters

journal homepage: www.elsevier.com/locate/cclet

# Ultrasensitive detection of microRNA-21 in human serum based on the confinement effect enhanced chemical etching of gold nanorods

Min Huang[a], Ru Cheng[a], Shuai Wen[a], Liangtong Li[a], Jie Gao[b], Xiaohui Zhao[c], Chunmei Li[a], Hongyan Zou[a,*], Jian Wang[a,*]

[a] Key Laboratory of Luminescence Analysis and Molecular Sensing (Southwest University), Ministry of Education, College of Pharmaceutical Sciences, Southwest University, Chongqing 400715, China
[b] Department of Biological and Chemical Engineering, Chongqing University of Education, Chongqing 400067, China
[c] The Ninth People's Hospital of Chongqing, Chongqing 400700, China

ARTICLE INFO

*Article history:*
Received 5 August 2023
Revised 21 November 2023
Accepted 4 December 2023
Available online 13 December 2023

*Keywords:*
Confinement effect
Hybridization chain reaction
Toehold-mediated strand displacement reaction
MicroRNA-21
Gold nanorods
Dark-field microscope

ABSTRACT

Natural enzymes, such as horseradish peroxidase (HRP), are a class of important biocatalysts with the high specificity, but their catalytic efficiency is usually unsatisfactory. Thus, the higher catalytic efficiency induced by the confinement effect is promising in optical sensing systems. In this work, a dark-field light scattering sensing platform was fabricated by the confinement effect of HRP from hybridization chain reaction (HCR) and then released to solution by the toehold-mediated strand displacement reaction (TSDR). Then, HRP catalyzed the 3,3′,5,5′-tetramethylbenzidine (TMB) to $TMB^{2+}$ with the assistance of hydrogen peroxide, which etched the gold nanorods (AuNRs) with the weakened light scattering. The single-particle assay was established based on the decreased light scattering intensity of AuNRs under dark-field microscope. The proposed assay revealed excellent analytical performance within a linear range from 25 pmol/L to 600 pmol/L, and a low limit of detection of 3.12 pmol/L. Additionally, it also manifested satisfactory recovery of miRNA-21 in human serum samples. The high sensitivity, excellent specificity, and universal applicability make this sensing platform promising for disease diagnosis.



MicroRNAs (miRNAs), as an important gene family that perform gene functions but do not encode proteins, guide RNA-induced silencing complex to specific messenger RNAs (mRNAs) to degrade or repress translation of mRNAs [1,2]. A complex regulatory network exists between miRNAs and their target genes [3], which is involved in abundant biological processes. The abnormal expression of miRNAs is associated with a large number of human diseases, especially cancers [4,5]. Therefore, the detection of miRNAs is essential for biological function research and disease diagnosis [6]. However, it is challenging due to the high sequence similarity [7] and low abundance [8] of miRNAs. Accordingly, it is highly desirable to develop sensitive and accurate sensing platforms for miRNAs detection [9,10].

So far, a variety of methods have been developed for miRNAs sensing, including colorimetry [11], fluorescence [12], electrochemistry [13], electrochemiluminescence (ECL) [14] and photoelectrochemistry (PEC) [15,16]. Colorimetry and fluorescence are convenient and rapid, but suffer from the poor sensitivity or stability, so signal amplification strategies are required [17–19]; electrochemistry, ECL and PEC are highly sensitive, but the electrode modification is complicated. Compared with the traditional analytical assays, dark-field microscopic (DFM) imaging technology offers many advantages, including low background and high sensitivity [20,21] due to the great spatial resolution [22], which has been received the widespread attention in the sensitive detection of microRNAs [23–25].

Usually, the noble metal nanoparticles with localized surface plasmon resonance (LSPR) are widely employed as optical probes because of the excellent high scattering efficiency [22,26]. Notably, the dark-field light scattering of nanoprobes is morphology-dependent, which can be effectively adjusted by etching [27], growth [28], assembly [29,30] and disassembly [31]. Especially, the asymmetrical etching of anisotropic nanomaterials is an available way to regulate the dark-field light scattering [32], which is able to avoid the false result induced by the aggregation. However, the effectively chemical etching of gold nanomaterials by $H_2O_2$ [33] or 3,3′,5,5′-tetramethylbenzidine (TMB) [34], is limited, which needs the enhancer to improve the etching efficiency. For example, our

* Corresponding authors.
*E-mail addresses:* zhy2013@swu.edu.cn (H. Zou), wj123456@swu.edu.cn (J. Wang).

https://doi.org/10.1016/j.cclet.2023.109379
1001-8417/

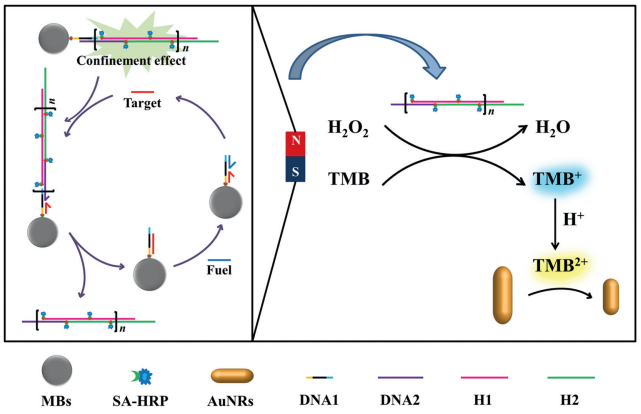


**Scheme 1.** The sensitive and selective sensing platform for miRNA-21 by the HCR and TSDR strategies under the dark-field light scattering microscope.

group improved the etching efficiency of $H_2O_2$ with $Fe^{3+}$ and KI [33]. Meanwhile, TMB is usually catalyzed by horseradish peroxidase (HRP) and acid to $TMB^{2+}$ to enhance the etching efficiency [35]. Furthermore, it has been found that $TMB^{2+}$ is provided with a stronger etching efficiency than $^{\bullet}OH$ produced by $H_2O_2$ due to the longer lifetime [34]. However, the catalytic efficiency of single HRP for TMB is not strong enough, which needs to further improve to catalyze TMB to $TMB^{2+}$ to etch gold nanomaterials. For example, Xu's group encapsulated HRP with liposomes to improve the catalytic efficiency of HRP for TMB to achieve the colorimetric detection of telomerase activity based on the effective etching of gold nanobipyramids [36].

In this work, HRP was modified on DNA strands, which was further confined by a hybridization chain reaction (HCR) [37,38] to improve the catalytic efficiency of HRP to further catalyze TMB to $TMB^{2+}$ to etch gold nanorods (AuNRs). Thus, a sensitive sensing platform for miRNA-21 detection was constructed based on HCR-mediated confinement effect of HRP. When in the presence of miRNA-21, HRP was released into solution *via* toehold-mediated strand displacement reaction (TSDR) (Scheme 1), leading to the effective etching of AuNRs with the weaker light scattering under DFM.

For the sensing platform, the construction of MBs-DNA-HRP complexes was essential. Herein, the DNA1-DNA2 hybrid strands were modified onto streptavidin magnetic beads (SA-MBs) by the specific biorecognition between biotin and streptavidin [39]. The 3′ end of DNA2 was complementary to a portion of H1, while H1 was also partially complementary to H2, so DNA2 could trigger HCR when H1 and H2 were present simultaneously. SA-HRP was likewise modified to the HCR product by the specific biorecognition between biotin and streptavidin. Owing to HCR, a higher amount of HRP was able to attach to the MBs-DNA, leading to a confinement effect to improve the catalytic efficiency of HRP. Moreover, the 3′ end of DNA1 was complementary to the target miRNA-21, so the HCR product modified with HRP would be displaced in the presence of miRNA-21. In contrast, the 5′ end of DNA1 was complementary to the fuel DNA, thus the fuel DNA was able to displace and assist the cycling of miRNA-21 by TSDR [23,40], leading to the signal amplification for the sensitive detection and endow the sensing platform with high specificity by magnetic separation. Furthermore, the magnetic separation facilitated the separation and collection of the released HRP. While HRP could catalyze TMB to blue $TMB^{+}$ with the assistance of $H_2O_2$, and it would transform into yellow $TMB^{2+}$ under acidic condition, which was able to etch AuNRs effectively [41]. The chemical etching led to the decrease in scattering intensity of AuNRs under DFM, which could be developed for the sensitive and specific detection of miRNA-21.

Feasibility of $TMB^{2+}$-mediated etching reaction was examined firstly. The as-prepared AuNRs exhibited strong longitudinal localized surface plasmon resonance at 667 nm and weak transversal localized surface plasmon resonance at 525 nm (Fig. 1A), corresponding to the longitudinal and transversal electron oscillation, respectively [42]. In the scanning electron microscope (SEM) images, AuNRs were uniform with a length of about 90 nm (Fig. 1B). Under DFM, AuNRs presented the strong red light scattering (Fig. 1C), which could be developed as the excellent optical probe for sensitive detection of biomarkers. It has been reported that $TMB^{2+}$ is a powerful etchant for AuNRs, leading to the remarkable changes in the morphological and optical features, which is advantageous to develop the sensitive sensing platforms [34]. As expected, the characteristic absorbance of $TMB^{2+}$ at 450 nm was gradually enhanced with the increasing HRP activity (Fig. S1A in Supporting information), which led to a gradual decrease in light scattering intensity of AuNRs (Fig. S2B in Supporting information), confirming the feasibility of $TMB^{2+}$-mediated chemical etching of AuNRs.

Polyacrylamide gel electrophoresis (PAGE) was used for the verification of HCR (Fig. 2A). All the DNA single-strands (DNA1 in lane 2, DNA2 in lane 3, H1 in lane 5 and H2 in lane 6) matched their molecular weights, and when DNA1 (lane 2) was incubated with DNA2 (lane 3), a strand with higher molecular weight was formed (lane 4), suggesting the hybridization of DNA1 and DNA2. If there was no trigger strand but only H1 and H2 were present, no strand with high molecular weight was found, suggesting that HCR product was not formed without trigger strand (lane 7). However, when DNA1-DNA2 was co-incubated with H1 and H2, HCR was triggered, which clearly presented a new band with much higher molecular weights (lane 8).

In addition, atomic force microscope (AFM) was applied to demonstrate the successful formation of HCR products. In the absence of the trigger strands, H1 and H2 could not react and there were only dispersed H1 and H2, so only a few of small and bright fragments were visible in the AFM image (Fig. 2B). While in the presence of the trigger strands, H1 and H2 could undergo the hybridization chain reaction to form long DNA products, so in addition to the small and bright fragments, the long chain products could also be clearly observed in the AFM image (Fig. 2C). The above results indicated the successful formation of HCR products, which supplied the possibility of confinement effect and signal amplification.

On the other hand, TSDR played the important role in signal amplification and the high specificity, which was verified with PAGE (Fig. S2 in Supporting information). Lane 1 was DNA marker, and lanes 2–5 with low molecular weights corresponded to DNA1, DNA2, miRNA-21 and fuel DNA, respectively. MiRNA-21 could successfully open the DNA1-DNA2 hybrid strand and release DNA2 (lane 9). In contrast, the fuel DNA could hardly open the DNA1-DNA2 hybrid strands (lane 10). However, when DNA1-DNA2 hybrid strands were co-incubated with miRNA-21 and fuel DNA, the band of DNA1-DNA2 completely disappeared and the band attributed to miRNA-21 appeared (lane 11), indicating that the fuel DNA was indeed able to assist the cycling of miRNA-21 by TSDR for signal amplification.

After feasibility validation was completed, MBs-DNA-HRP complexes were constructed. The success of the construction could be verified by measuring the zeta potential of the products at each step (Fig. 3). The SA-MBs were the products of chemically immobilizing streptavidin onto magnetic microspheres, endowing them with negative charge. The zeta potential was decreased after the modification of DNA1-DNA2 on SA-MBs, and then continued to decrease after the formation of HCR products, and finally decreased to the lowest after the modification of SA-HRP, indicating the successful construction of MBs-DNA-HRP complexes.

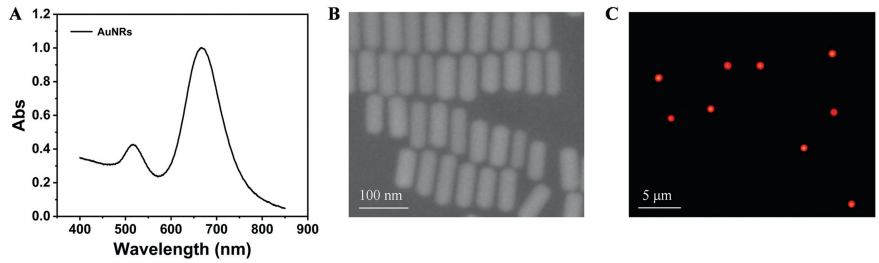


**Fig. 1.** Characterization of AuNRs. (A) UV–vis absorption spectrum of AuNRs. (B) SEM image of AuNRs. (C) Dark-field microscopic imaging of AuNRs.

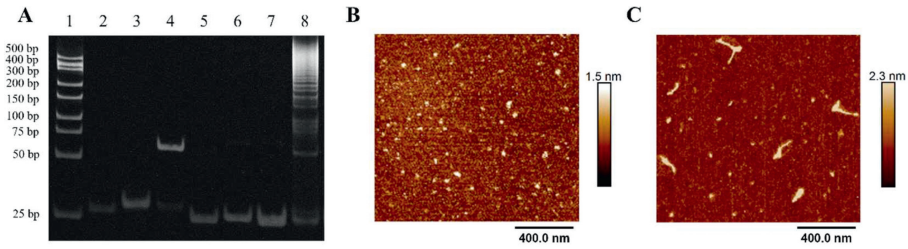


**Fig. 2.** Verification of HCR. (A) PAGE analysis of HCR. Lane 1, DNA marker; lane 2, DNA1; lane 3, DNA2; lane 4, DNA1+DNA2; lane 5, H1; lane 6, H2; lane 7, H1+H2; lane 8, DNA1+DNA2+H1+H2. The concentrations of all nucleic acid sequences were 1 μmol/L except that H1 and H2 were 4 μmol/L. The 12% PAGE was operated at 120 V for 60 min. (B) AFM image of HCR products in the absence of DNA1-DNA2. (C) AFM image of HCR products in the presence of DNA1-DNA2. Conditions: DNA1-DNA2, 48 nmol/L; H1, 210 nmol/L; H2, 210 nmol/L; time of HCR, 4 h.

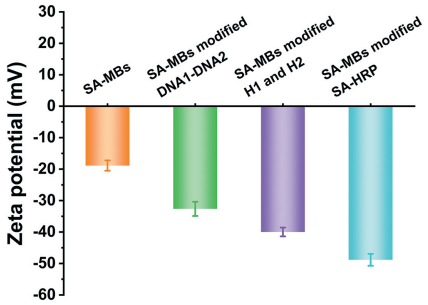


**Fig. 3.** Characterization of MBs-DNA-HRP complexes. Zeta potential of SA-MBs, SA-MBs modified DNA1-DNA2, SA-MBs modified H1 and H2 and SA-MBs modified SA-HRP. Conditions: SA-MBs, 0.17 mg/mL; DNA1-DNA2, 48 nmol/L; poly-T, 130 nmol/L; H1, 210 nmol/L; H2, 210 nmol/L; time of HCR, 4 h; SA-HRP, 13 μL.

In order to achieve the optimal analytical performance, some important factors in this work were investigated. DNA1-DNA2 complex was critical for the variation of the scattering intensity of AuNRs since it was acted as the initiator of HCR and the aim of TSDR. When the concentration of DNA1-DNA2 complex was low, it failed to form a large number of HCR products for the confinement effect, while the too high DNA1-DNA2 concentration resulted in large steric hindrance of TSDR. The result confirmed that the optimal concentration of DNA1-DNA2 was 48 nmol/L (Fig. S3A in Supporting information). Moreover, poly-T was designed to satiate the excess streptavidin sites on MBs, while too much poly-T would compete with DNA1-DNA2, so 130 nmol/L of poly-T was chosen for the following work (Fig. S3B in Supporting information). In order to form more HCR products, sufficient H1 and H2, as well as adequate reaction time were necessary, so 210 nmol/L of H1 and H2 and 4 h of reaction time were optimal (Figs. S3C and D in Supporting information). In addition, the sufficient SA-HRP allowed the HCR products to be fully modified for sufficiently etching of AuNRs, while too much SA-HRP led to a high background, so 13 μL of SA-HRP was appropriate (Fig. S3E in Supporting information). The concentration of fuel DNA and the duration of TSDR were essential for signal amplification. Low concentration and short time were not conducive to target cycling, while too high concentration or long time might lead to false positive results. As a result, 200 nmol/L of fuel DNA and 60 min of reaction time were optimal (Figs. S3F and G in Supporting information).

Under the optimal experimental conditions, the scattering intensity of AuNRs gradually decreased as increasing concentration of miRNA-21 (Fig. 4A) due to the chemical etching of AuNRs. The SEM images showed the transversal length of AuNRs was shortened (Fig. S4 in Supporting information), leading to the weakened light scattering ($\Delta I$). This method showed a good linear relationship range from 25 pmol/L to 600 pmol/L (Fig. 4B), which could be expressed as $\Delta I = 112.1\ c_{\text{miRNA-21}} + 3471$ ($R^2 = 0.9986$) and the limit of detection (LOD) was 3.12 pmol/L, presenting an equal or even higher sensitivity compared with some previously reported methods for miRNA-21 detection (Table S2 in Supporting information).

Due to the high sequence similarity and low abundance of miRNAs, selectivity and anti-interference ability were evaluated to verify the specificity and accuracy of miRNA-21 detection. The mismatched sequences of miRNA-21 were employed to evaluate the selectivity and anti-interference ability. Even if the concentration of each mismatched nucleic acid was 10 times higher than that of miRNA-21, the decrease in scattering intensity of AuNRs was not significant (Fig. 4C), suggesting the high specificity of miRNA-21 detection. Besides, the simultaneous presence of miRNA-21 and mismatched nucleic acids also hardly affected the scattering intensity of AuNRs (Fig. S5 in Supporting information), suggesting the excellent specificity and accuracy of the assay.

In order to validate the performance of the developed sensing platform for detecting miRNA-21 in practical samples, human serum samples containing miRNA-21 were employed. Different concentrations of miRNA-21 (100 pmol/L, 300 pmol/L and 500 pmol/L) were added to human serum samples for recovery test. The recoveries ranged from 99.46% to 101.66% (Table 1), demonstrating the potential of this sensing platform for disease diagnosis.

In this work, the sensitivity was improved by the single-particle analytical technique and the dual signal amplification strategies, including the HCR and TSDR. Especially, the confinement effect from HCR played the key role in sensitivity improvement. To

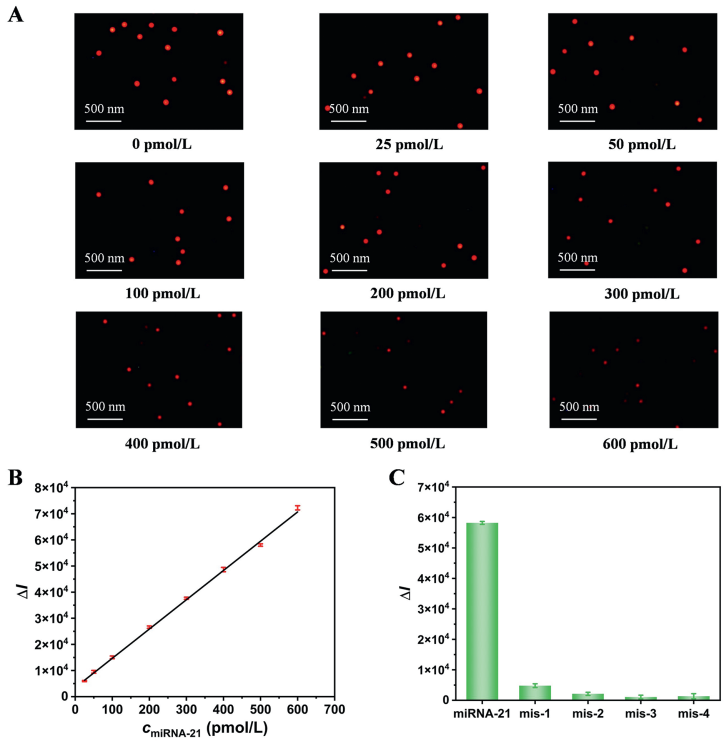


**Fig. 4.** Analytical performance of miRNA-21. (A) Dark-field microscopic imaging of AuNRs at various concentrations of miRNA-21. (B) Linear relationship between the variation of scattering intensity and the concentration of miRNA-21. (C) Selectivity of the proposed assay. Conditions: MBs, 0.17 mg/mL; DNA1-DNA2, 48 nmol/L; poly-T, 130 nmol/L; H1, 210 nmol/L; H2, 210 nmol/L; time of HCR, 4 h; SA-HRP, 13 μL; fuel DNA, 200 nmol/L; time of TSDR, 60 min; miRNA-21, 500 pmol/L; mismatched nucleic acids, 5 nmol/L; $H_2O_2$, 1 mmol/L; TMB 1 mmol/L; hydrochloric acid, 0.1 mol/L; AuNRs, 125 pmol/L.

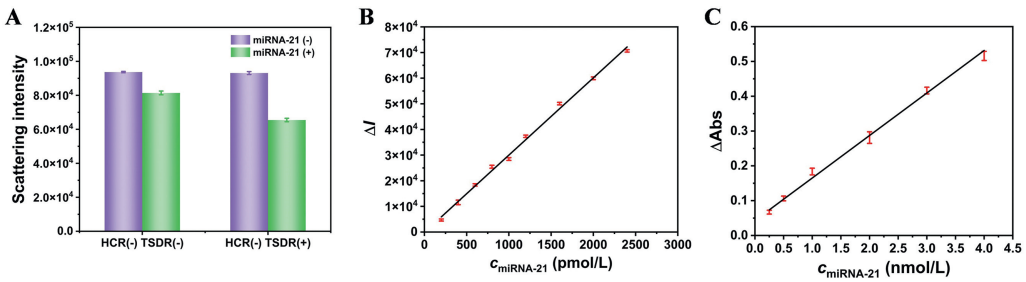


**Fig. 5.** Comparison of sensitivity. (A) Variation of scattering intensity in the absence of HCR signal amplification strategy. (B) Linearity of the method in the absence of TSDR signal amplification strategy. (C) Linearity of the colorimetry based on $TMB^{2+}$. Conditions: MBs, 0.17 mg/mL; DNA1-DNA2, 48 nmol/L; poly-T, 130 nmol/L; H1, 210 nmol/L; H2, 210 nmol/L; time of HCR, 4 h; SA-HRP, 13 μL; fuel DNA, 200 nmol/L; time of TSDR, 60 min; $H_2O_2$, 1 mmol/L; TMB 1 mmol/L; hydrochloric acid, 0.1 mol/L; AuNRs, 125 pmol/L.

**Table 1**
Determination of miRNA-21 in human serum samples.

| Samples | Added (pmol/L) | Average found (pmol/L) | Average recovery | RSD ($n=3$) |
|---|---|---|---|---|
| 1 | 100.00 | 101.66 | 101.66% | 0.33% |
| 2 | 300.00 | 298.39 | 99.46% | 1.01% |
| 3 | 500.00 | 501.52 | 100.30% | 3.04% |

demonstrate the confinement effect contribution from HCR, the sensitivity was compared. Remarkably, when in the absence of H2, HCR product could not be formed, leading to a weak decrease in scattering intensity of AuNRs even though the concentration of miRNA-21 was as high as 4 μmol/L, regardless of the TSDR signal amplification strategy was introduced or not (Fig. 5A). However, when HCR was introduced, the weakened light scatting ($\Delta I$) was much higher than that without HCR even if the concentration was much lower than 4 μmol/L (Fig. 4B). It highly suggested that the confinement effect contribution from HCR played key role in improving the sensitivity for miRNA-21 sensing, which was functioned as one of signal amplification strategies. Furthermore, TSDR signal amplification strategy was not induced if fuel DNA was absent, leading to a low sensitivity in a linear range from 200 pmol/L to 2400 pmol/L (Fig. 5B), which could be expressed as $\Delta I = 30.12 c_{\text{miRNA-21}} - 121.6$ ($R^2 = 0.9959$) and the LOD was 17.53 pmol/L. The above results fully demonstrated that both HCR and TSDR were effective for improving the sensitivity. Additionally, TSDR strategy released HCR-confined HRP to the solution in the presence of microRNA-21 and then to further improve to catalyze TMB to $TMB^{2+}$ to etch gold nanomaterials, which endowed the sensing platform with the high specificity. Moreover, instead of dark-field microscopic imaging technology, colorimetry based on $TMB^{2+}$ was also considered. The variation of absorbance ($\Delta$Abs) showed a linear relationship range from 0.25 nmol/L to 4 nmol/L (Fig. 5C), which could be expressed as $\Delta\text{Abs} = 0.1221 c_{\text{miRNA-21}} + 0.04305$ ($R^2 = 0.9949$) and the LOD was 0.15 nmol/L. It was evident that the sensitivity of the single-particle dark-field light scattering technique was superior compared with

the colorimetry. In brief, the integration of two signal amplification strategies and the application of dark-field microscopic imaging technology jointly improved the sensitivity of this proposed assay.

In summary, a sensitive and accurate sensing platform for detecting miRNA-21 was constructed based on a single-particle dark-field light scattering technique and dual signal amplification strategy. HCR allowed more SA-HRP to be modified to MBs-DNA, leading to a remarkable confinement effect for enhancing the sensitivity, while TSDR assisted the cycling of miRNA-21 and endowed the sensing platform with the high specificity. In addition, the application of dark-field microscopic imaging technology enabled the assay with more sensitive result than colorimetry. Moreover, the employment of magnetic separation made the separation of DNA extremely simple and efficient to avoid the false result. Besides, the nucleic acid sequences can be adjusted for the analysis of other nucleic acid biomarkers, which is universally applicable. In one word, the high sensitivity, excellent specificity, and universal applicability enable this sensing platform promising for disease diagnosis.

## Ethical statement

This work contains human blood samples from Southwest University, which operated according to the ethical standards of the Ethics Committee of Southwest University Hospital (No. 202304181610).

## Declaration of competing interest

The authors declare that they have no known competing financial interests or personal relationships that could have appeared to influence the work reported in this paper.

## Acknowledgments

It is highly appreciated for the financial supported from the National Natural Science Foundation of China (No. 22174115), and the Graduate Education and Teaching Reform Research Project of Chongqing (No. yjg223038), as well as the Fundamental Research Funds for the Central Universities (No. SWU-XDJH202321).

## Supplementary materials

Supplementary material associated with this article can be found, in the online version, at doi:10.1016/j.cclet.2023.109379.

## References

[1] M. Jinek, J.A. Doudna, Nature 457 (2009) 405–412.
[2] J. Winter, S. Jung, S. Keller, et al., Nat. Cell Biol. 11 (2009) 228–234.
[3] F. Li, Y. Zhou, H. Yin, et al., Biosens. Bioelectron. 166 (2020) 112476.
[4] M. Ha, V.N. Kim, Nat. Rev. Mol. Cell Biol. 15 (2014) 509–524.
[5] T. Jet, G. Gines, Y. Rondelez, et al., Chem. Soc. Rev. 50 (2021) 4141–4161.
[6] S.Y. Chen, J.J. Zhao, I.Y. Sakharov, et al., Biosens. Bioelectron. 203 (2022) 114053.
[7] S. Joo, U.J. Lee, H.Y. Son, et al., ACS Sens. 7 (2022) 3409–3415.
[8] Z. Liu, N. Xie, J. Li, et al., Anal. Chem. 95 (2023) 4529–4535.
[9] S.Y. Chen, J.J. Zhao, C.H. Xu, et al., Anal. Chem. 93 (2021) 9218–9225.
[10] L. Yang, J. Fang, J. Li, et al., Anal. Chim. Acta 1143 (2021) 157–165.
[11] K. Shahsavar, E. Shokri, M. Hosseini, Microchim. Acta 189 (2022) 357.
[12] Z. Sun, Y. Tong, X. Zhou, et al., ACS Omega 6 (2021) 34150–34159.
[13] J. Zhang, M.F. Hou, G.Y. Chen, et al., Chin. Chem. Lett. 32 (2021) 3474–3478.
[14] M.Y. Wang, W.J. Jing, L.J. Wang, et al., Biosens. Bioelectron. 226 (2023) 115116.
[15] L. Jiang, J. Du, H. Xu, et al., Anal. Chem. 95 (2023) 1193–1200.
[16] J.F. Chang, W.X. Lv, J.H. Wu, et al., Chin. Chem. Lett. 32 (2021) 775–778.
[17] C.H. Xu, S.Y. Chen, S.Q. Hu, et al., Anal. Chem. 95 (2023) 11061–11069.
[18] M. Bai, F. Chen, X.W. Cao, et al., Angew. Chem. Int. Ed. 59 (2020) 13267–13272.
[19] R.M. Li, F.Z. Li, Y.P. Zhang, et al., Anal. Chem. 95 (2023) 3848–3855.
[20] H. Wang, C.H. Xu, W. Zhao, et al., Anal. Chem. 93 (2021) 10727–10734.
[21] S.M. Wang, H. Wang, W. Zhao, et al., Chin. Chem. Lett. 34 (2023) 108053.
[22] J.J. Liu, S. Wen, H.H. Yan, et al., Anal. Chem. 95 (2023) 1169–1175.
[23] H.H. Yan, Q. Zhang, R. Cheng, et al., ACS Appl. Bio Mater. 4 (2021) 3469–3475.
[24] J.J. Liu, H.H. Yan, Q. Zhang, et al., Anal. Chem. 92 (2020) 13118–13125.
[25] Q. Zhang, H.H. Yan, R. Cheng, et al., Biosens. Bioelectron. 201 (2022) 113942.
[26] P.F. Gao, G. Lei, C.Z. Huang, Anal. Chem. 93 (2021) 4707–4726.
[27] W. Xu, M. Ouyang, H. Luo, et al., New J. Chem. 46 (2022) 15473–15480.
[28] Y. Zhao, X.Y. Gao, H. Wang, et al., Anal. Chem. 91 (2019) 15988–15992.
[29] H.H. Yan, M. Huang, F. Zhu, et al., Anal. Chem. 95 (2023) 3968–3975.
[30] S. Chen, W. Wang, S. Xu, et al., Anal. Chim. Acta 1187 (2021) 339162.
[31] D. Zhang, K. Wang, W. Wei, et al., Anal. Chem. 93 (2021) 9521–9530.
[32] Z. He, L. Zhang, G. Peng, et al., J. Anal. Test. 5 (2021) 350–359.
[33] J.J. Liu, H.H. Yan, D. Yuan, et al., Talanta 219 (2020) 121203.
[34] X.F. Yang, W. He, Y.F. Li, et al., ACS Appl. Nano Mater. 5 (2022) 1484–1490.
[35] Z. Chen, C. Chen, H. Huang, et al., Anal. Chem. 90 (2018) 6222–6228.
[36] D. Wang, Y. Zhang, X. Zhao, et al., Sensor. Actuat. B: Chem. 296 (2019) 126646.
[37] Y. Zhao, C. Lu, X.E. Zhao, et al., Biosens. Bioelectron. 208 (2022) 114215.
[38] L.N. Huang, Z.J. Zhong, Q.J. Lu, et al., J. Anal. Test. 6 (2022) 36–43.
[39] M. Hou, D.G. He, H. Wang, et al., Chin. Chem. Lett. 33 (2022) 3183–3187.
[40] N. Wang, Y.J. Jiang, K.H. Nie, et al., Chin. Chem. Lett. 34 (2023) 107906.
[41] S. Yadav, J. Satija, Nanoscale Adv. 4 (2022) 3928–3939.
[42] C.J. Murphy, H.H. Chang, P. Falagan-Lotsch, et al., Acc. Chem. Res. 52 (2019) 2124–2135.